10.2514/6.2022-2257

AIAA 2022 SciTech Forum, 3-7 January 2022, San Diego, California

Plasma-Assisted Burner Array Development using Cyclotronic Arc-Plasma Actuators

Joseph W. Zimmerman*, and David L. Carroll†
CUA, Champaign, Illinois 61822

and

Georgi K. Hristov‡, and Phillip J. Ansell§
University of Illinois at Urbana-Champaign, Urbana, Illinois 61801

Magnetically-guided atmospheric arc devices were applied to provide plasma-excitation to premixed methane-air flames. Researchers have recently applied similar technology to study vortex generation for aerodynamic flow control, and the scaling and driver circuits used for those devices has been leveraged in the presented work. To provide a plasma-exited volume, an arc is produced in the gap of coaxial electrodes placed within the field of a strong rare-earth magnet. Due to drift motion in the magnetic field, the charged particles experience Lorentz force which causes the arc filament to sweep about the center of the coaxial electrodes. To observers, this takes on the apparent form of a plasma "disc" at the tip of the coax. The technique is applied to flame holding by integrating flow channels in the dielectric spacers of the coax, through which fuel and oxidizer are injected and mixed in the rotating plasma filament. The use of zero voltage switching circuits operating in the 70-80 kHz range to introduce plasma power in the flame zone is reported, with these circuit modules being powered by low voltage DC supplies (e.g., 24 V). The enhanced mixing effect of the plasma-excitation technique was demonstrated through high-speed imaging and schlieren. Gas analyzers were used to measure the reduction in the unburnt CO level above the lean flame zone when the plasma system was engaged. The methodology for sizing the coaxial plasma burners for natural gas combustion is presented. An array of plasma-assisted burners was demonstrated using this technique, with lean methane flow rates (ϕ = 0.76) corresponding to available heat release between 46 and 138 kW.

Nomenclature

AC	=	alternating current
AHR	=	available heat release
B	=	magnetic field
BFS	=	blue flame sensor
CAPA	=	cyclotronic arc plasma actuator
CAPAC	=	cyclotronic arc plasma assisted combustor
CRT	=	cathode ray tube
CUA	=	CU Aerospace, LLC
d_Q	=	quenching distance (methane)
d_T	=	quenching diameter (methane)
DBD	=	dielectric barrier discharge
DC	=	direct current

* Director, Plasmadynamics at CU Aerospace, Associate Fellow AIAA.
† President of CU Aerospace, Fellow AIAA.
‡ Graduate Research Assistant, Department of Aerospace Engineering, Student Member, AIAA
§ Assistant Professor, Department of Aerospace Engineering, Senior Member AIAA.

f = frequency (for driver circuit)
F = force, Lorentz force
FAR = fuel-to-air equivalence ratio
fps = frames per second
HV = high voltage
I = current
ID = inner diameter
LBO = lean blow-off limit
MHD = magnetohydrodynamics
OD = outer diameter
PAC = plasma-assisted combustion
PGP = plasma gas processing
PIV = particle image velocimetry
Re = Reynolds number
RPM = revolutions per minute
S_u = burning velocity
SLM = standard liters per minute
SWaP = size, weight, and power
UIUC = University of Illinois at Urbana-Champaign
UV = ultraviolet
V = voltage
V_∞ = free stream velocity
VG = vortex generator
ZVS = zero voltage switching
ϕ = fuel-to-air equivalence ratio

I. Introduction

Recent work demonstrated the capability of plasma-assisted combustion techniques to extend the lean-flame limits of methane combustion in configurations such as free jets and swirled chamber flows. By application of plasma-excitation to the flame zone (e.g., by microwave heating), electronically-excited molecules and atoms are introduced, enabling flame maintenance in flow conditions that are normally unstable. If this technology is properly matured, optimized, extended to operation with infrastructure-compatible fuels, and commercialized, it has the potential for lowering fuel consumption as well as reducing pollution in a variety of applications.

The current work investigates the innovation of applying plasma-excitation to fuel and oxidizer streams using magnetically-guided atmospheric arcs. Researchers have made recent advances in applying similar technology to vortex generation for aerodynamic flow control [Ansell, 2019; Hristov 2019]. In this approach, an arc is produced in the gap of coaxial electrodes placed within the field of a strong rare-earth magnet. Due to drift motion in the magnetic field, the charged particles experience a Lorentz force which causes the arc to sweep about the center of the coaxial electrodes. To observers, this takes on the apparent form of a plasma "disc" at the tip of the coax. Modification of this technology to flame holding is straightforward, by replacing the dielectric spacers of the coax with injection tubes through which fuel and oxidizer are introduced and mixed in the rotating constricted glow discharge. Further flame control is envisioned through timing of the arc pulse width and frequency to counter flow instabilities in combustion chambers, or by introducing enhanced mixing with proper selection of arc current and magnetic field strength. Variations on this general arc-magnet concept are also appealing for flame stabilization in chambers and high-speed flow, as well as atmospheric-pressure gas processing.

The objective of the research is to apply magnetically-guided arcs to enhance the combustion of methane, conduct preliminary research to improve understanding of the plasma-flame interaction, and investigate the influence of the new plasma-assisted approach on flame stability limits in combustion chamber flows. Some goals of the experimental investigations are as follows: (1) development of an arc-magnet flame-holder testbed, including a pulse generation circuit operating from a zero-voltage switching source, and a plasma-assisted flame-holder with optical access for flame diagnostics, (2) analysis of the plasma technique effect on flame constituents, applying laser-induced fluorescence, spectroscopy of nitrogen states, and mass spectrometry to characterize chamber exhaust, (3) examination of the impact of the technique on flame stability, and (4) preliminary prototype design, including scaling, pulse circuit

development, and examination of critical aspects to promote long life cycle of the arc-magnet devices, such as material selection, electrode erosion, and thermal design to avoid magnet degradation. Alternative plasma flow-control applications are also envisioned, such as plasma gas processing (PGP) of carbon dioxide. Potential commercial markets for applying this technology are high-efficiency gas-turbine engines with improved turn-down ratio, advanced commercial and residential furnaces and boilers, and compact on-demand hybrid (gas-electric) water heaters.

II. Experimental Setups and Operating Conditions

A. Typical Test Circuit and Data Acquisition for PAC System with Coaxial Actuator

The typical actuator bench test configuration investigated in the recent tests is shown in Figure 1.

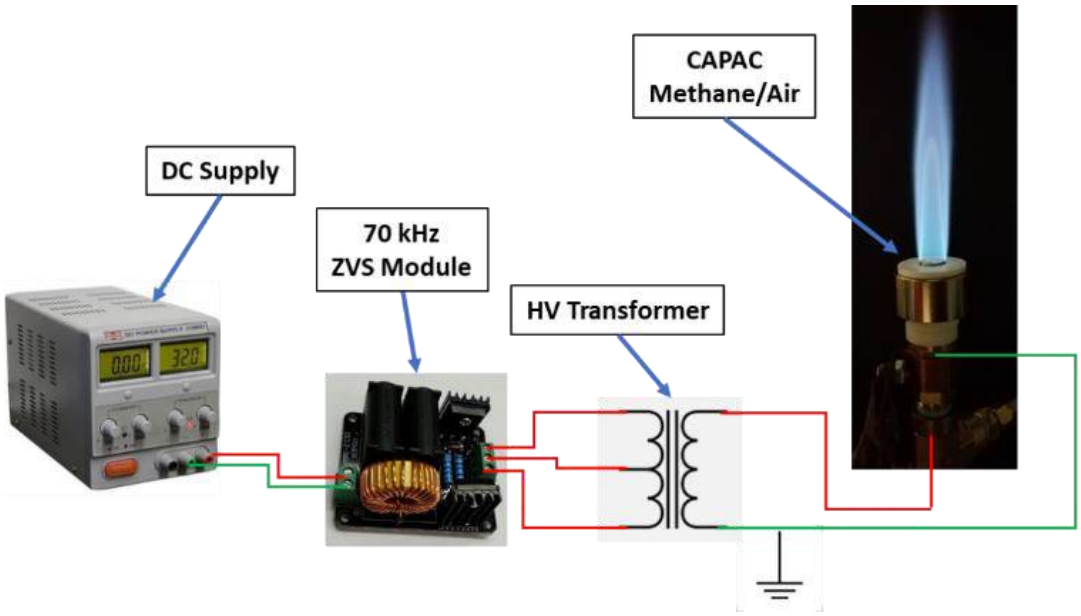

Figure 1. CAPAC Bench Test Equipment: DC Supply / ZVS Driver Circuit Module / High Voltage Transformer and CAPAC Burner.

The CAPAC (cyclotronic arc-plasma actuator combustor) methane/air setup utilized two flow controllers, one flow meter, one thermocouple, three pressure sensors, a band-pass filtered FDS100 Si photodiode to monitor blue flame emissions, and an in-line ammeter/voltmeter device. Thermocouples were interfaced using a NI USB-TC01 K-type thermocouple DAQ from National Instruments. Typical measurements were in the flow exhaust, between 19°C and 800°C in the CAPAC experiments, depending on the configuration.

Flow controllers were applied to meter and control methane and air flow mixture into the CAPAC burners. A GFC17 Aalborg Flow Controller, rated up to 2 SLM of nitrogen, was used for metering methane and nitrogen flows. A GFC37 Aalborg Flow Controller, rated up to 20 SLM of nitrogen, was used for metering pressurized air. Each flow controller requires 12-15VDC power to operate, accepts an input voltage of 0-5VDC and outputs a voltage signal of 0-5VDC. The input and signal voltages each are directly proportional to either the ratio of the desired or current flow (respectively) to the maximum flow rating of the controller. An additional FMA1724 Omega Flow Meter rated up to 20 SLM was used to meter pressurized air or argon in secondary flows. The flow meter requires 12-15VDC power to operate and outputs a voltage signal of 0-5VDC, directly proportional to the ratio of flow to the maximum flow rating.

Pressure sensors were placed to monitor the fuel and air lines. The pressure sensors used were all analog output Automotive Grade Pressure Sensors (AG Pressure Sensors) with a range of -14.5psi to 30.0 psi, relative to atmospheric pressure. Each required 5VDC to operate and outputs between 0.5VDC and 4.5VDC, proportional to the measured pressure.

A Thorlabs FDS100 silicon photodiode was used as a sensor for blue flame emissions. The emission from the PAC burners was collected through a low-pass filter with 500 nm cutoff, and focused onto the FDS100 photodiode which was amplified monitored in with the DAQ system. This was used to log the behavior of the flame emissions with changes in flame mode and shape.

The ammeter/voltmeter which monitored DC power to the ZVS module consisted of a bank of power resistors in line with the return path for monitoring current, and a simple voltage divider in parallel with the module for monitoring the voltage. The ammeter functions by reading the voltage across the two 1 Ω resistors in parallel as current travels from the ZVS driver back to the power common, while the voltmeter functions by reading the voltage drop between the positive and common poles of the power source at a point between the 3.3 kΩ and 10 kΩ resistors. Similar circuitry was used to measure the total DC power into the CAPAC array system.

B. Coaxial Configurations for Burners or Flow Reactors

The bench test actuator studied here is shown in Figure 2. The plasma reactor consists of a coaxial flow tube formed by dielectric material (alumina), with a center electrode contained in the center dielectric tube, and a (grounded) electrode sheath surrounding the outer dielectric tube. Near the exit of the coaxial tube, a ring magnet is positioned outside the outer electrode circumference to supply *B*-field in the region between the coaxial electrodes. The strength of the magnet was validated by measuring the *B*-field at the top surface of the ring magnet (half way between the inner and outer radii) using a 1D gaussmeter. The level of the *B*-field at the surface of the magnet was typically 5 kG. The magnet sizes vary for the range of configurations being developed; for a 0.5" flow tube, a 1.5" OD magnet was typical. For purposes of this study, these devices are referred to as cyclotronic arc plasma-assisted combustors (CAPACs), as the general approach is similar to the cyclotronic arc plasma actuators (CAPAs) developed by Ansell *et al.* [Ansell, 2019].

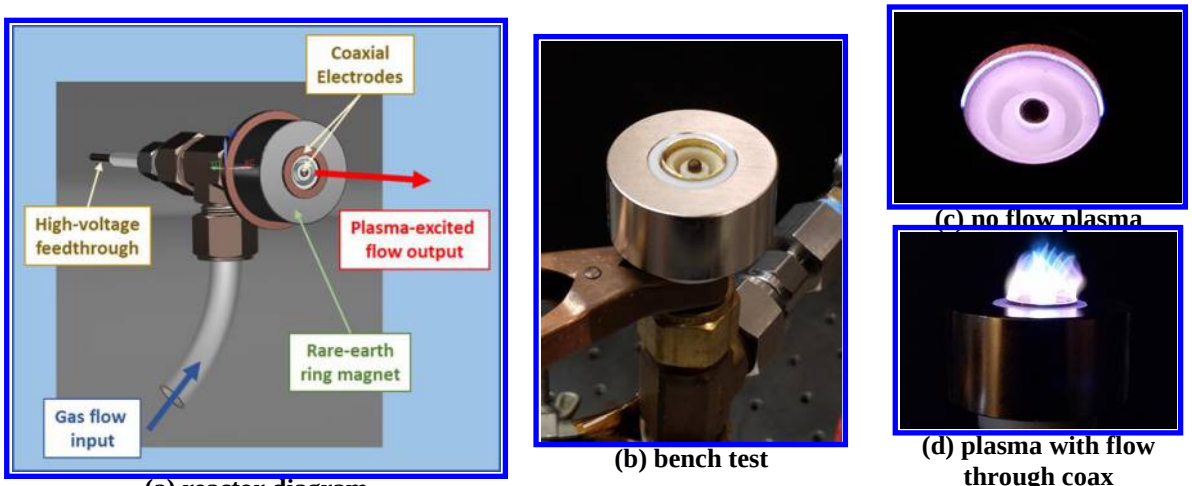

Figure 2. Sketch of cyclotronic arc plasma assisted combustor (CAPAC) reactor for PAC Studies

C. Plasma-Assisted Burner Design and Operation Modes

Figure 3 graphically summarizes the various stability constraints considered in design of a Bunsen type burner, sized for operation in methane-air mixture. Various data points are overlaid on Figure 3 which correspond to burner tube sizes, flow rates, and operating conditions of CAPAC devices constructed and tested with methane-air flames.

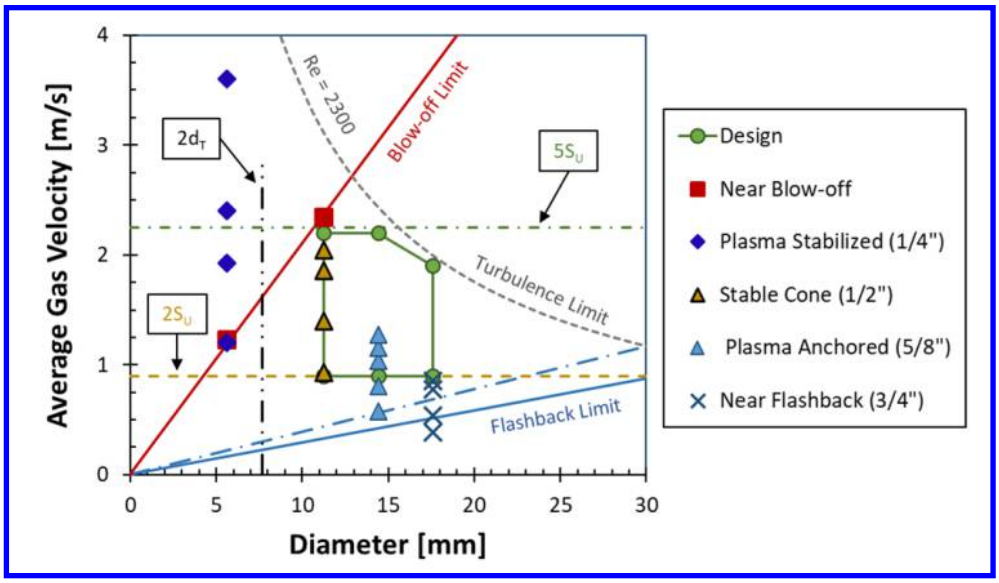

Figure 3. Parameters Determining the Region of Stable Operation for a Bunsen Burner (Modified recreation of the chart in Fig. 3.9 from [Barnard and Bradley, 1985])

The various constraint lines in Figure 3 correspond to upper limits for Blow-Off of the flame, lower limits for Flashback, an upper limit related to transition to turbulent flow (at Re = 2300), as well as approximate limits for operation of a stable cone between twice and five times the burning velocity S_U, which for methane-air mixture is a maximum of 0.45 m/s (0.43 m/s for propane-air) [Barnard and Bradley, 1985]. A parameter d_T is also defined called the quenching diameter which is 1.54 times the quenching distance for methane in air, d_Q = 2.5 mm; this distance corresponds to the minimum distance between two plates which allows a flame to propagate. Based on the various constraints, the green box with circular data points labelled "Design" corresponds to the practical limits for stable operation of a Bunsen-type burner. The CAPAC burners developed in this study are essentially Bunsen style burners, modified to include coaxial electrodes with a center electrode feedthrough along the tube centerline, and the flow tube itself serving as an outer electrode; the diagonal dashed blue line is a modification to the flashback limit accounting for the change in velocity due to the coaxial geometry. The remainder of the data points in Figure 3 correspond to actual operating conditions applied in initial studies of CAPAC devices (devices detailed in

Table 1), operating with pressurized methane and air bottle sources, with air flow typically in the range of 5 to 15 SLM and methane up to 1.4 SLM. Four regimes were identified based on the scale of each burner from left to right in this chart: (1, blue diamonds) **Plasma Stabilized** operation corresponding to cases with CAPAC-1G where a lean flame was maintained using plasma, (2, gold triangles) **Stable Cone-Shaped Flame** corresponding to CAPAC-1B operated as a Bunsen burner with its center electrode removed, (3, blue triangles) **Plasma-Anchored Flame** cases corresponding to CAPAC-1H configured with a 0.625" tube outer electrode, and (4, blue X) **Near Flashback** operation, corresponding to CAPAC-1H configured with a 0.75" tube outer electrode. Here below is a more detailed description of each of these cases:

- **Case 1, Plasma Stabilized:** This corresponds to a list of cases where 3x CAPAC-1G modules were configured for operation as an array from a single DC power supply. The total air flow rate varies from 5 to 15 SLM, and the fuel-to-air (FAR) equivalence ratio was ϕ = 0.76. These cases could only be stabilized with plasma. If fuel flow was increased to $\phi > 1$, the flames operated as stable cones (without plasma), or as anchored flames (with plasma).
- **Case 2, Stable Cone-Shaped Flame:** With the center electrode lowered in the device, CAPAC-1B operates as a typical straight tube Bunsen burner, having a cone-shaped inner core flame (Λ-shape) and diffuse outer cone flame which changes size and shaped depending on flow rate and equivalence ratio, ϕ.
- **Case 3, Plasma-Anchored Flame:** This condition is fundamentally similar to Case 2, with the unactuated flame being similar to a cone-shaped Bunsen flame. However, when the rotating plasma arc filament is activated, the inner cone is modified and anchors to the bluff body wake of the coax (V-shape). At lowest flow rates, the addition of plasma causes operation inside the tube.

- **Case 4, Near Flashback:** In this condition the flame operates as a marginally stable cone-shaped flame at high flow rates, and anchors inside the tube at lower flow rates. Activation of plasma causes the flame to anchor inside the tube except for at the highest flow rates where it operates as a V-shaped flame anchored to the coax center electrode.

Various photographs were taken of the Λ-shaped anchored flames over a range of methane and air flow rates (in cases without plasma power). The approximate angle 2θ of the inner cone (due to emissions from intermediates at the flame front) was used to estimate the burning velocity $S_u = V\sin\theta$, defining it as the gas velocity component normal to the cone overlaid in the captured images. The maximums near $\phi = 1$ are similar to various measurements found in the literature for methane, and confirmed that the fuel/air flow system was operating as expected. Various examples of this technique can be found in the literature (for example [Londoño, 2013]).

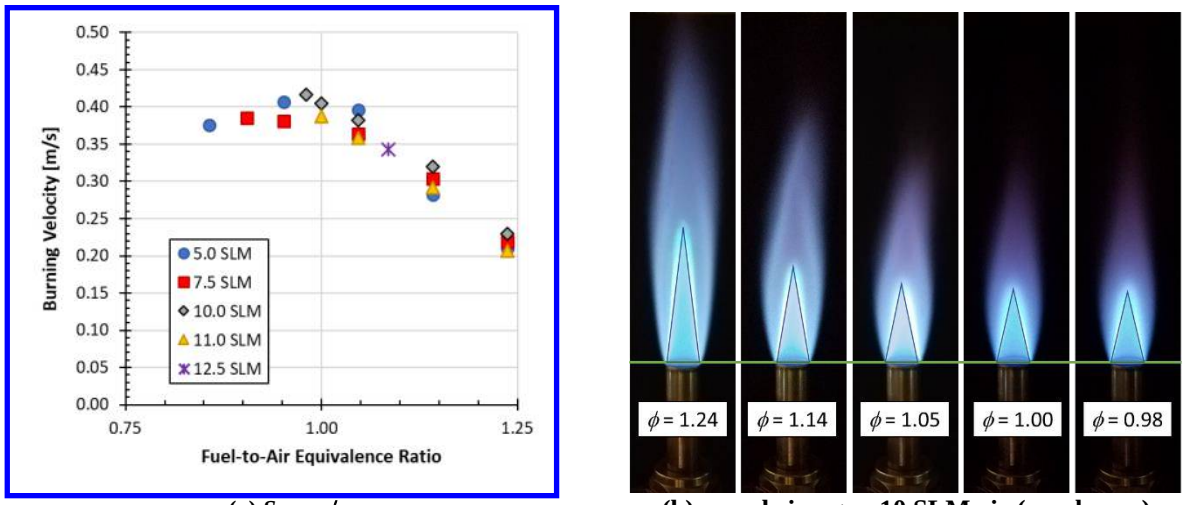

(a) S_u vs. ϕ **(b) sample images, 10 SLM air (no plasma)**

Figure 4. Burning Velocities Approximated from Λ-shaped Anchored Flames in Methane-Air Mixtures (no plasma)

D. Optical Diagnostics

This study also made use of compact spectrometer to monitor the plasma filament emissions and the flame emissions. One system applied is a compact Vis-NIR spectrometer module which is configured to measure emissions from oxygen excited states. To test the viability of this approach an Ocean Optics USB4000 Vis-NIR spectrometer (Figure 5) was applied to monitor plasma-excited oxygen emissions from the plasma filament generated with the zero-voltage switching circuit. This spectrometer has a 3648 pixel array and is setup with a #6 grating (NIR, 1200 g/mm) and a 5 μm slit to view over the range of 713-985 nm. This system allows capture of the emissions from various oxygen species in the flow downstream of the RF discharge including $O_2(b^1\Sigma)$ at 762 nm, $O(3p^5P)$ at 777 nm and $O(3p^3P)$ at 844 nm, Figure 6. The O_2(b) electronically-excited state at 1.63 eV originates from electron impact of ground state oxygen. The atomic emissions originate from electronically excited states at 10.74 and 10.99 eV above ground state which are produced predominately from electron impacts with dissociated oxygen atoms.

During this study, a method was devised to measure the NIR emission of the plasma filament, remove background structure from N_2 emissions, and then model the distribution of oxygen atom emissions (777, 844, 926 nm lines) to determine the temperature based on a Saha-LTE model (using the NIST LIBS online model as a reference). This method gave results in the range of 3600 to 3700 K (example case in Figure 6).

(a)

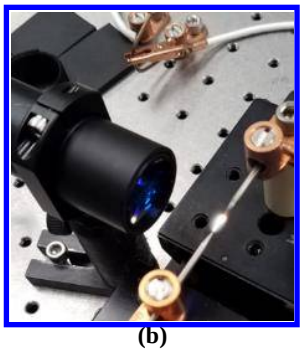

(b)

Figure 5: Ocean Optics compact modular USB4000 spectrometer (a) and collection optics viewing plasma filament (b)

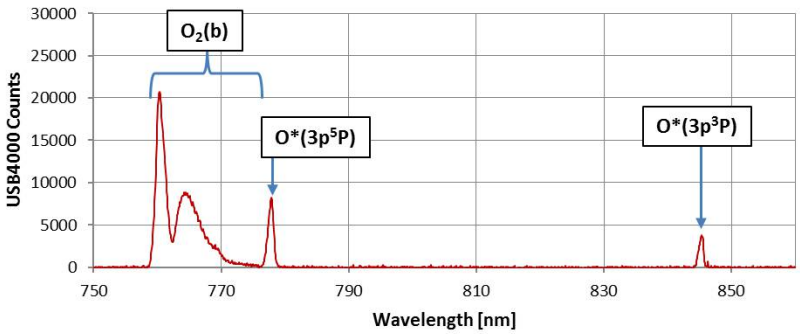

(a)

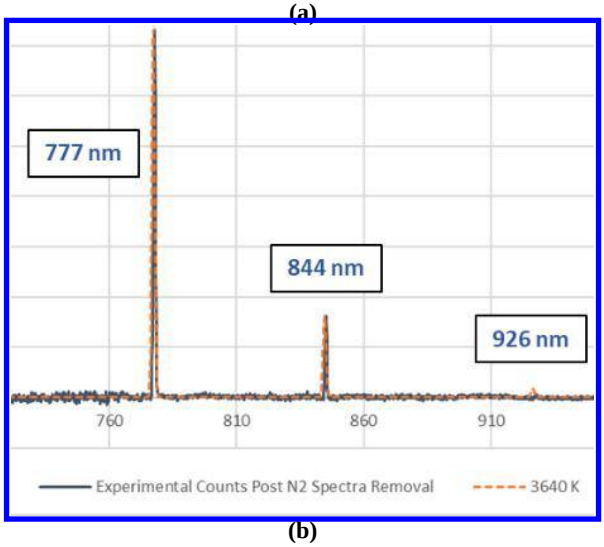

(b)

Figure 6: Emission spectra of electronically-excited oxygen states (O_2(b) at 762 nm, and O* at 777, 844 and 926 nm: (a) downstream of a flowing low temperature RF discharge with operating conditions of 12.5:25 mmol/s O_2:He, 12.5 Torr, and 800 W RF, and (b) in the arc filament in ambient air using the ZVS circuit driver at 72 kHz (with N_2 bands removed by optical filters and modeling algorithm).

A B&W Tek UV-Vis spectrometer was applied to monitor emissions from the flames, primarily emissions from C_2 bands in the flame cone. Figure 7 shows examples of emissions from propane and butane flames, where 516 nm and 564 nm bands have the highest intensity.

(a)

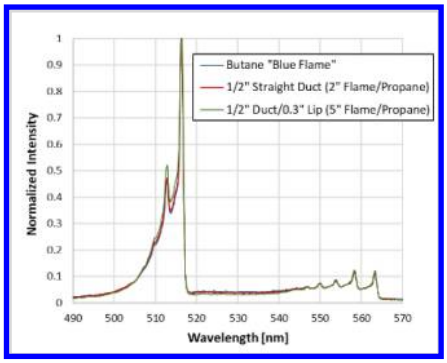

(b)

Wavelength [nm]	(v', v'')	Typical strength	Observed
438.2	(2, 0)	vw	Yes
473.7	(1, 0)	vs	Yes
516.5	(0, 0)	vs	Yes
563.6	(0, 1)	s	Yes
619.1	(0, 2)	w	Out of range

(c)

Figure 7. C_2 Swan Band Emissions from Hydrocarbon Flames with B&W Tek UV-Vis Spectrometer: (a) propane flame operating in CAPAC, (b) comparison of butane and propane torch emissions, (c) C_2 bands observed

For monitoring the status of the flame, a blue flame sensor (BFS) was applied, making use of a fast Si diode filtered in the 350-500 nm band to measure intense emissions from intermediates such as C_2 and CH. This diagnostic was used to monitor the status of the flame, and monitored shifts in intensity as the flame height was varied in the viewing volume. During experiments where fuel and air flow were varied, it was used to monitor cases where blow-off or flash back limits were reached (resulting in loss of signal). The intensity was monitored as fuel-to-air ratio was swept to characterize flame behaviors while gas analyzer measurements were also being made (e.g., CO ppm levels).

Schlieren data were acquired for air flow only through the CAPAC-1B, and for premixed flames of various fuel-air ratios. A standard two-mirror schlieren setup, seen in Figure 8 was used. This configuration included two parabolic mirrors, a point source of light, a vertical knife edge, and a high-speed camera. A Photron Mini AX200 high-speed camera equipped with a photographic lens was used to acquire schlieren images of the flow at a frame rate of 6400fps. The camera had an image size of 1024 × 1024 pixels and was operated at a shutter speed of 1/6400s.

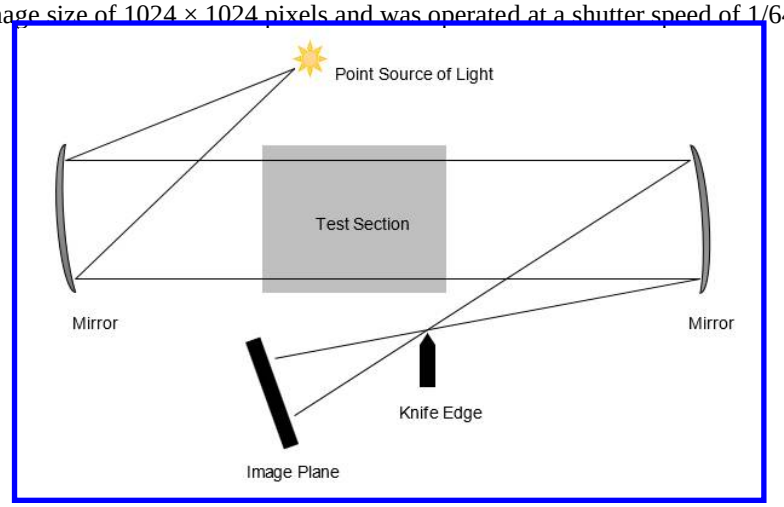

Figure 8. A schematic of the Schlieren setup.

E. Application of Gas Analyzers

The present study made use of gas analysis techniques to study the exhaust flow above the flame zone. One technique applied the sampling of the exhaust by a Stanford Research Systems mass spectrometer. While this allowed the detecting of the buildup in carbon dioxide and water levels in the exhaust and corresponding removal of methane fuel from the flow, the technique could not detect any useful information about unburnt constituents (e.g., CO or NO levels).

For monitoring of CO levels in the exhaust, a Kane-May SGA91 combustion analyzer was applied, typically making measurements in the exhaust at a height of six inches (150 mm) above the burner. This device is one designed for diagnosing the CO levels in exhaust of commercial heaters in the heating and ventilation industry.

III. Bench Testing of Plasma-Assisted Combustors

A. Configuration Studies for CAPAC Burners

For the demonstration effort, a straight forward feedthrough design was created, making use of readily available off-the-shelf parts and material stock, and applying modifications and machining which could be readily performed with various machine shop tools. The configuration which was applied for the majority of recent testing is shown in Figure 9. This basic design is comprised of standard brass fittings, standard 0.5” brass tubing, alumina dielectric tubing, super-conductive copper rod, PTFE dielectric flange and spacers, and a standard N42 grade neodymium magnet. The 0.625” NPT tee fitting which serves as a plenum could be readily adapted to the methane/air flow system described in above, or it could be adapted to a Venturi system (e.g., using an off-the-shelf propane torch as a feed system). The simple coaxial feedthrough arrangement allows for modifications to the positioning of the electrode and the ring magnet by repositioning of the feedthrough “antenna” or repositioning the magnet. The effective electrode gap, and the flow geometry could be made by modifications to the outer electrode tube using either a thicker wall, or

a modification to the flow exit diameter. Thus, with this simple design, various configurations and modifications could be tested, using a 72 kHz ZVS circuit to provide plasma power.

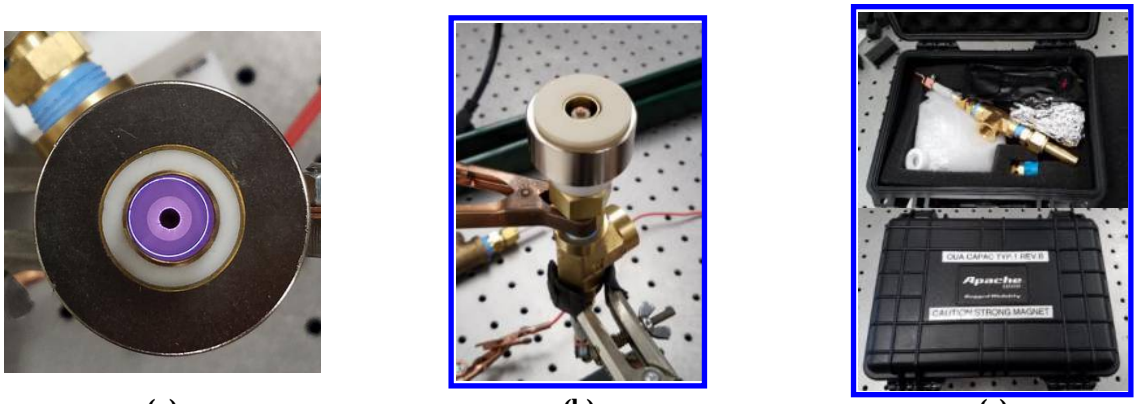

(a) **(b)** **(c)**

Figure 9. CAPAC Type 1 Revision B: (a) top view with plasma in no-flow case, (b) supported in lab stand during initial testing with ZVS driver, and (c) packaged for transport to UIUC for further flow visualization tests

Different burner configurations were explored by varying the plasma discharge position along the magnet height, therefore, changing the magnetic field strength that provided the Lorentz forcing. Three main configurations, shown in Figure 10, were considered. The discharge rotation for all cases was first visualized using a Photron Mini AX200 high-speed camera operated at frame rates from 6,400 fps to 50,000 fps. The first configuration (Figure 10a) placed the discharge in the middle of the magnet height where the magnetic field was the strongest. The discharge was located upstream away from the burner outlet but had the largest discharge rotation speeds of up to 24,000 rpm. The other two configurations placed the discharge at the burner outlet but achieved significantly lower rotation speeds of up to 5,200 rpm. The difference between these configurations was the polarity of the magnetic field, and therefore the direction of rotation. The magnet position in Figure 10b placed the discharge in the same magnetic field polarity as the configuration in Figure 10a. In contrast, the configuration in Figure 10c placed the magnet sufficiently far away from the discharge such that the magnetic field polarity was reversed.

The first magnet configuration, which provided the highest rotation rate, was chosen for further study considering that it would provide the largest swirling and excitation of the flow. The fluid dynamic interactions of the plasma were studied using high speed visualization. The rotation of the discharge at different input power settings and different air flow rates through the coaxial configuration were imaged. Figure 11 summarizes the data. It is immediately evident that the axial flow and its interaction with the discharge has a noticeable influence on the rotation speed of the filament. The axial air flow lifts up the end of the filament that attaches to the outer ground electrode while the other inner end remains anchored to the high voltage electrode. Thus, the discharge rotation shifts from a flat horizontal plane in the no axial flow case to a conical surface in the axial flow case. This shifts the discharge with respect to the magnetic field, therefore reducing the Lorentz force and the rotation rate. Little variation in the rotation rate was observed across the range of axial air flow rates tested. Stereo-PIV measurements were also conducted with this apparatus to quantify the velocity fields, vorticity, and helicity developed in the flow field above the actuator [Hristov, 2022].

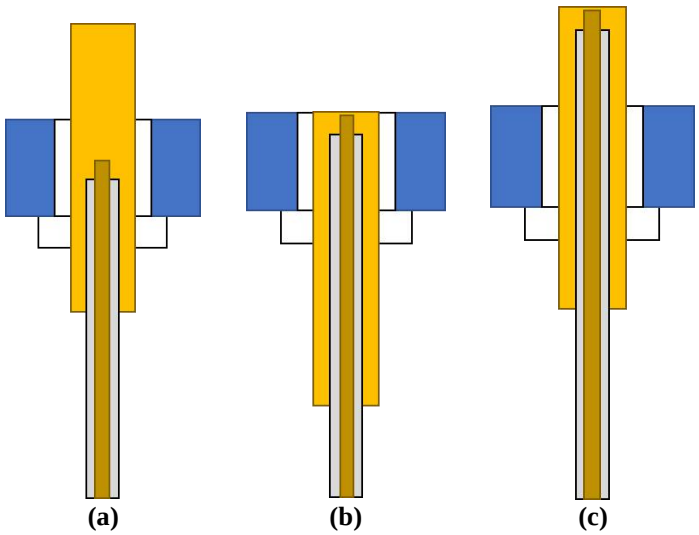

Figure 10. CAPAC-1B magnet configurations: a) Discharge at the middle of the magnet height; b) Discharge flush with the top surface of the magnet; c) Discharge away from the magnet surface.

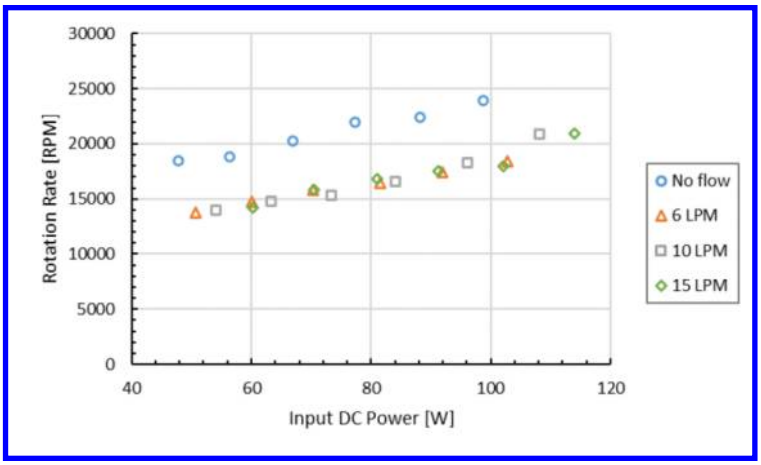

Figure 11. Rotation rate of the discharge as a function of input DC power and air flow rate.

In addition to this configuration, a few other similar devices were created for bench testing, Figure 12 (CAPAC-1E) and Figure 13 (CAPAC-1H). CAPAC-1H could be operated with various outer electrodes (various flow tube diameters). Another smaller module was also built and multiples of these were used to build an array system (CAPAC-1G). Designs are described in

Table 1. All of the versions discussed here applied pressurized air and methane sources. The datapoints in Figure 3 span the range of operation which could be achieved with these burners and the flow system described above; the larger designs could potentially accommodate higher flow rates than those applied in the current study. The sizing of the coaxial burner with flow rate is crucial, in that operation with too large of a diameter for a given flow rate resulted in a flame operating near flashback, and the addition of the plasma filament in this case resulted in a plasma-excited flame inside the flow tube. An arrestor system was applied in the feed system to avoid issues with flames propagating upstream of the burner.

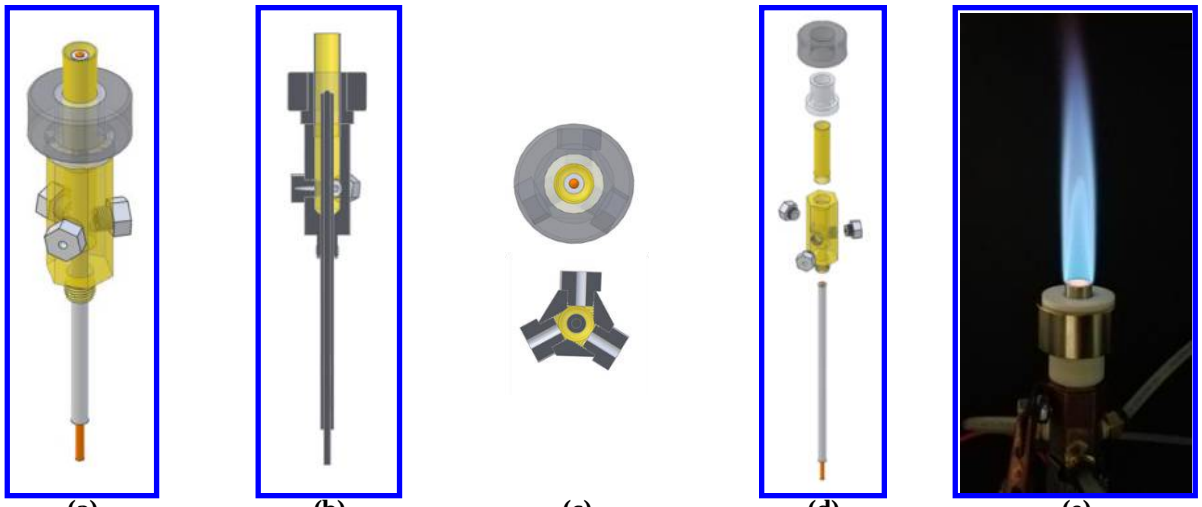

Figure 12. CAPAC Type 1 Revision E: (a) isometric (b) side-view sectional cutaway, (c) top view of magnet and sectional cutaway of plenum, (d) exploded view, and (e) image of fuel-rich methane-air flame with inner and outer cone and plasma excitation

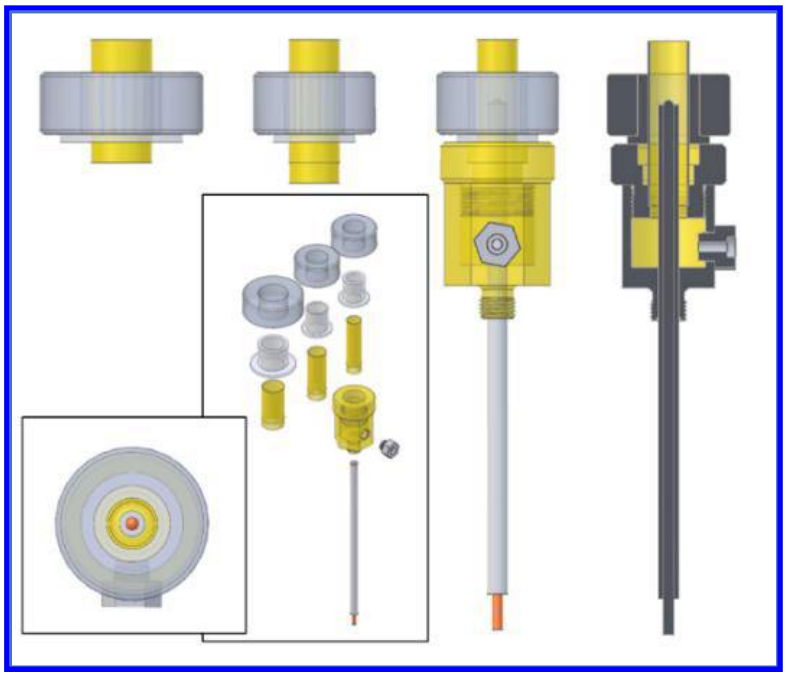

Figure 13. CAPAC Type 1 Revision H: (lower left inset) top view, (center inset) isometric view of various parts, (top) side view of various magnet/tube combinations, and (right) side-view sectional cutaway

Table 1. CAPAC Designs Built for Initial Configuration Studies

CAPAC #	Features	Magnet Diameter [in.]	Tube Size [in.] (mm)	Coaxial Gap [in.] (mm)	Use
CAPAC-1A	OTS Fittings, alumina flow tube	1.5	0.5 (12.7)	0.1585 (4.03)	Initial Concept Demonstration
CAPAC-1B	OTS Fittings, brass flow tube/electrode	1.5	0.5 (12.7)	0.1585 (4.03)	Characterization studies
CAPAC-1E	3-port Plenum	1.5	0.5 (12.7)	0.1585 (4.03)	Characterization studies
CAPAC-1G	Compact, OTS Fittings	1.0	0.25 (6.4)	0.0798 (2.03)	Reduced capacity Applied in array
CAPAC-1H	Variable gap and flow tube size	Reconfigurable	Varies	Varies	Gap size Flow volume

B. Schlieren Measurements with Plasma-Assisted Combustion in Methane-Air Mixtures

Examples of a fuel-rich and lean flames were shown in Figure 14 and Figure 15 respectively, where the flame behaviors can be observed in greater detail. In order to isolate the effects of the plasma swirling from the effects on the flame chemistry, the rotation of the discharge was eliminated by removing the magnet. Removing the swirling was evident in the increases in lateral extent in the diffusion cone of the fuel-rich flames (e.g., 5 SLM of air and 14% fuel). However, the lack of swirling was most noticeable in the lean flames, where the flame would anchor itself down in the burner tube, at the location of the discharge. In this case, the flame would no longer be axisymmetric, and it would lean to one side depending on the discharge location. It is evident from the color and shape that the non-swirled flames lack swirling stabilization and uniform flame enhancement.

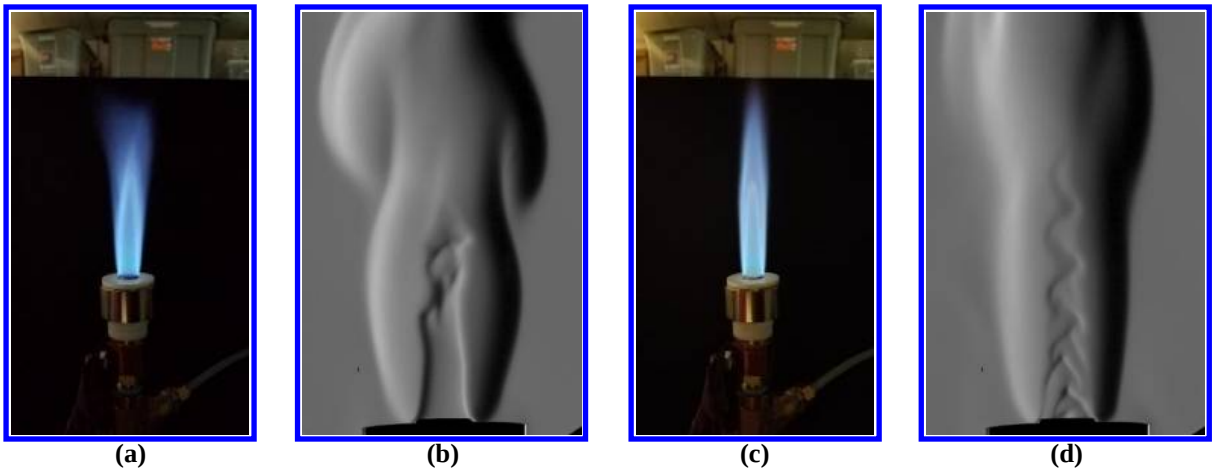

(a) **(b)** **(c)** **(d)**

Figure 14. Fuel-rich flame at 5 SLM air flow and 18% CH4: a) unactuated flame photograph; b) schlieren image of the unactuated flame; c) actuated flame photograph; d) schlieren image of the actuated flame

(a) (b) (c) (d)

Figure 15. Lean flame at 5 SLM air flow and 7% CH4: a) unactuated flame photograph; b) schlieren image of the unactuated flame; c) actuated flame photograph; d) schlieren image of the actuated flame

C. Carbon Monoxide Measurements with Gas Analyzer

The Kane-May SGA91 CO single gas analyzer was used to monitor the CO in the flow above the flame in a variety of cases. For the cases shown in Figure 16a without plasma, the CO probe was placed six inches above the upper surface of the burner. The data shows that the CO levels are relatively low over a range of fuel-to-air (FAR) equivalence ratios, but at $\phi < 0.9$ the CO levels rise as fuel-to-air ratio is decreased; also, higher total flow rate (higher velocity) results in higher CO levels at the measurement point. Over the same range of ϕ, the blue flame sensor, or BFS (a filtered Si photodiode), current passes through a maximum between $\phi = 1.0$ and $\phi = 1.2$. Figure 17 (5 SLM air) and Figure 18 (10 SLM air) show data logging CO and BFS current as methane is varied, and plasma is turned on and off.

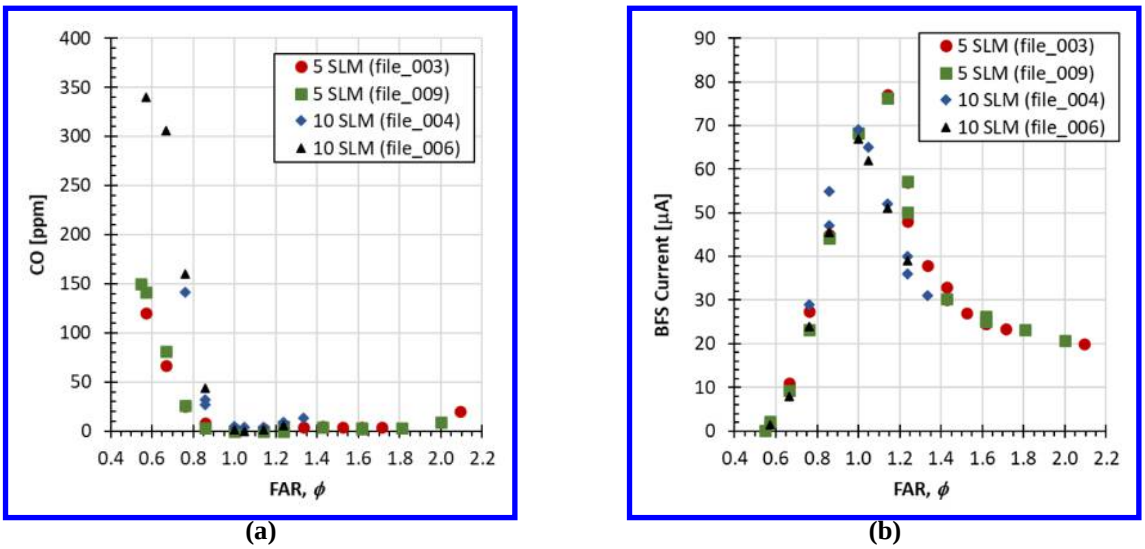

(a) (b)

Figure 16. Carbon Monoxide 6" above flame and blue flame emission intensity as a function of fuel-to-air equivalence ratio for <u>baseline cases without plasma</u> in CAPAC-1B: (a) Kane-May SGA91 CO measurements, and (b) 350-500 nm filtered "blue flame sensor" current measurements

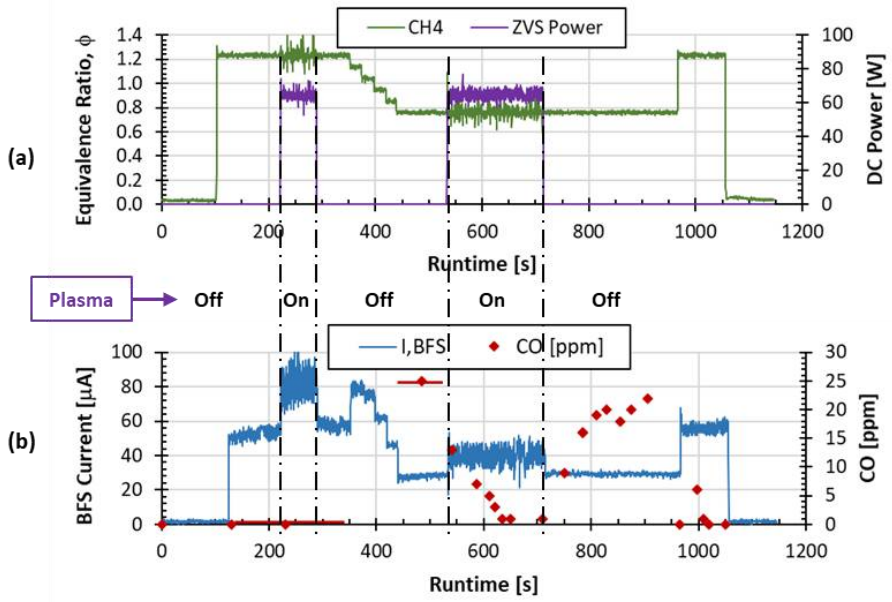

Figure 17. Comparison of CO measurement and blue flame sensor as a function of time for 5 SLM air and varied methane: (a) ϕ and DC power to the ZVS, and (b) blue flame sensor current and CO

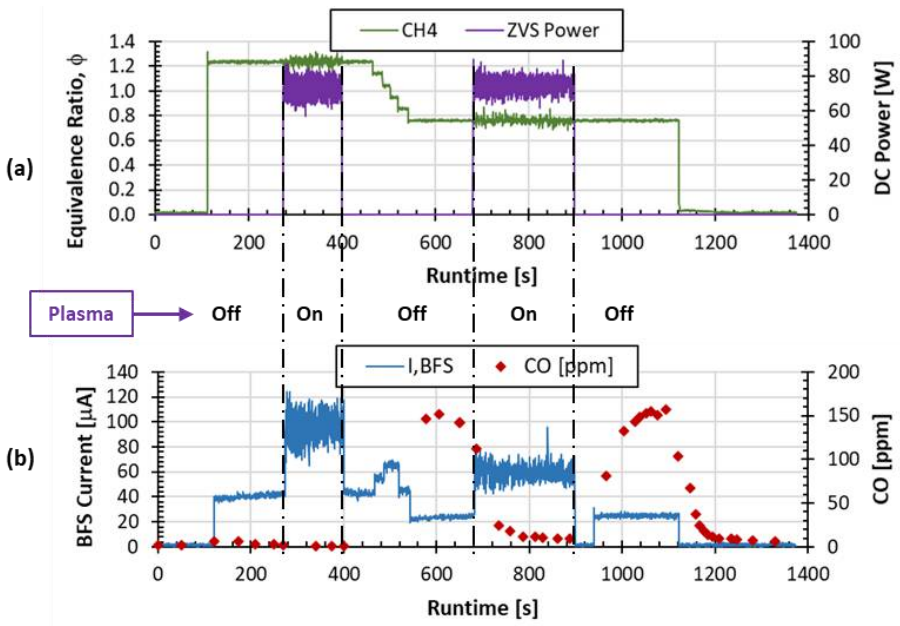

Figure 18. Comparison of CO measurement and blue flame sensor as a function of time for 10 SLM air and varied methane: (a) ϕ and DC power to the ZVS, and (b) blue flame sensor current and CO

The data in Figure 17 and Figure 18 indicate clearly that the CO ppm measurement is reduced (to nearly zero) at $\phi = 0.76$ when the plasma is turned on. In both cases, the plasma being turned on at $\phi = 1.24$ (fuel-rich) and $\phi = 0.76$ (fuel-lean) leads to higher emission in the zone above the CAPAC flame-holder; the blue flame sensor (BFS) views the zone immediately above the CAPAC upper surface and is filtered in the 350-500 nm band to measure intense emissions from intermediates such as C_2 and CH. In the fuel-lean case, the increase in BFS current is due to the increased C_2 and CH in the viewing volume due to a more energetic flame. In the fuel-rich case the increased BFS current is due to an acceleration of the flame front (faster effective burning velocity) due to the plasma excitation and swirling, and the anchoring of the inner flame cone in a V shape such that the C_2 intermediate zone is focused above

the coax bluff body. This anchoring effect is fundamentally similar to what was observed in microwave excitation cases [Rajasegar, 2017; Zimmerman, 2016].

D. UV-Vis Spectroscopy Measurements

When the plasma is turned on in the CAPAC for cases with an existing stable flame, there is a significant change in the structure of the blue flame cone, and the character of the change depends on the flow rate and the fuel-to-air ratio. Figure 14 and Figure 15 show this with color digital photos and schlieren imaging. This corresponds to a change in the emissions from intermediates, especially C_2 which make up the blue-green emissions in the inner cone of the methane-air flame. The emission of C_2 Swan system ($A^3\Pi_g \rightarrow X^3\Pi_u$) from the CAPAC flame was collected with a 35 mm lens focused on a 200 μm fiber optic connected to the B&W Tek compact UV-Vis spectrometer, with a typical integration time of 1 second.

A variety of behaviors were observed in comparing the emissions measurements in Figure 19. First, it is observed that in the fuel-rich $\phi = 1.24$ case (Figure 19a) the v' = 0 C_2 emissions (516.5 nm and 563.6 nm bands) are reduced when the plasma is turned on while the weaker v' = 1, 2 emissions (438.2 nm and 473.7 nm) remain at similar intensity. In the $\phi = 1.14$ case (Figure 19a), all of the C_2 emissions are significantly decreases when plasma is turned on.

As fuel level is lowered the flame anchors in the coax (without or with plasma) and a relatively weak broad emission band is observed at 525 nm which is from CO oxidation (flame bands) in the outer cone of the flame. In these cases, there is not a significant change in the shape of the CO emission, although CH is seen (near 438 nm) in the $\phi = 0.86$ case when plasma is turned on, and in the $\phi = 0.76$ case the CO – O emission decreases slightly when plasma is turned on.

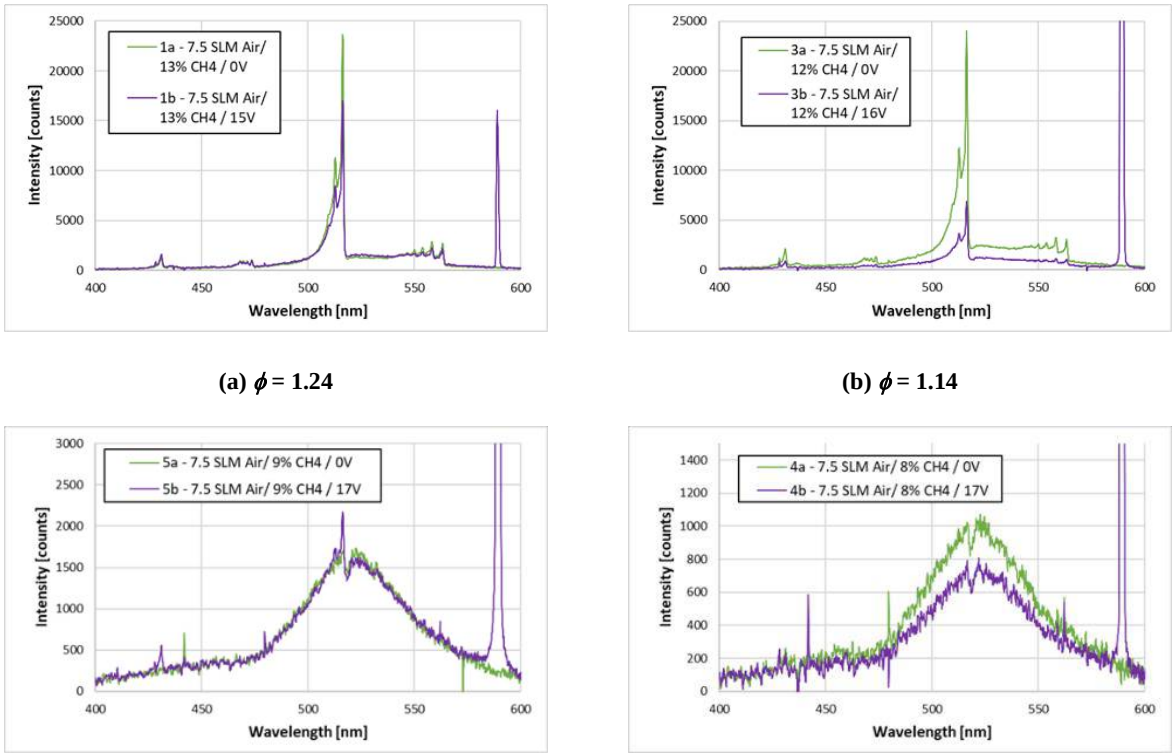

(a) $\phi = 1.24$ **(b) $\phi = 1.14$**

(c) $\phi = 0.86$ **(d) $\phi = 0.76$**

Figure 19. UV-Vis Spectrometer Measurements (400 to 600 nm) for 7.5 SLM air and varied methane fuel, without (light green curves) and with plasma (dark purple curves)

These cases indicate the modification of the flame chemistry by the plasma, where the major effect is the anchoring of the flame to the coax bluff body which is also evident in various photos. It is possible to model the

temperature of the 516.5 nm and 563.6 nm, however there is no indication of any strong variation of the distribution in the various cases, and the buildup of the complex band at 525 nm in the outer cone is problematic, especially with the poor resolution of the compact spectrometer. In blue flame cases (e.g., $\phi = 1.1$, cone-shaped flame), the modeled rotational temperature (using PGOPHER software) was similar to the expected methane-air stoichiometric flame temperature (2222 K), while the vibrational temperature was about 5000 K based on the distribution of states.

In all four cases shown in Figure 19a-d, the most obvious effect is the well-known sodium D-line emission at 589 nm, which is observed strongly in the cases where plasma is added. The excitation of this emission is most likely due to three-body recombination of hydrogen atoms in reactions forming H_2 and H_2O. The measurement of the D-line of sodium is commonly used in the study of metal spectra in hydrogen-oxygen-nitrogen flames, and is due to contributions of the recombination of hydrogen atoms into hydrogen molecules and H + OH into water molecules, where the recombination of these radicals excites the sodium atoms which then emit on the resonance lines at 589 nm [Gaydon, 1974]. The associated recombination reactions which excite sodium are:

$$Na + H + H \rightarrow Na^* + H_2$$

and

$$Na + H + OH \rightarrow Na^* + H_2O$$

The presence of this chemiluminescence mechanism with the addition of plasma in the CAPAC is an indication that the plasma filament enhances breakdown of CH_4 and O_2 increasing the number of energetic radicals. The source of the sodium in this experiment is unknown, although it is potentially a contaminant in the methane gas bottle.

E. Assembly and Testing of an Array of CAPAC Devices

A set of three CAPAC-1G burner components were built, and these were assembled into an array and supplied high-frequency AC with a bank of ZVS circuits and CRT HV transformers, all powered by a single DC power supply module (not shown). This array was tested to measure power requirements for various air flow rates (shared gas supply from a single plenum), and then also tested with methane-air flames, both in fuel-rich (stable) modes, and in non-stable modes where plasma was required to generate a flame. During these initial tests, multimeter modules with digital readouts for DC voltages and currents to each ZVS board were monitored. Figure 20 shows the setup of the CAPAC-1G array.

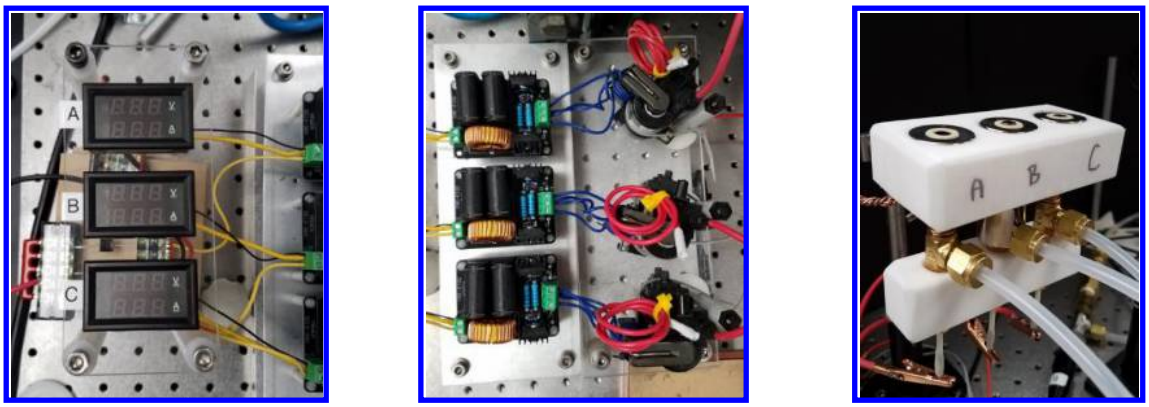

(a) **(b)** **(c)**

Figure 20. CAPAC Array Test: (a) Multimeter Modules, (b) ZVS boards and CRT transformers, (c) 3x CAPAC-1G burners mounted in PTFE blocks for testing with methane-air premix

Figure 21 shows cases for increasing total flow rate and $\phi = 0.76$. For the range of flow rates shown in, the available heat release (AHR) in the methane flow varies from 46 kW to 138 kW, while the DC power used by the ZVS circuits varies from 0.163 to 0.195 kW, and therefore the plasma power input is significantly lower than the flame power.

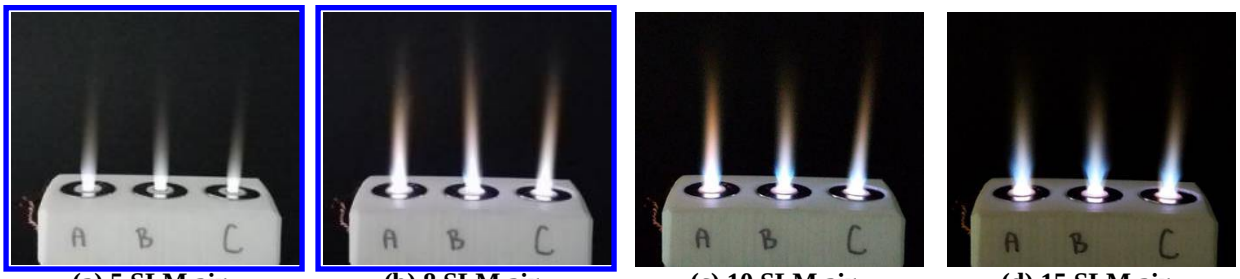

(a) 5 SLM air, $\phi = 0.76$ **(b) 8 SLM air, $\phi = 0.76$** **(c) 10 SLM air, $\phi = 0.76$** **(d) 15 SLM air, $\phi = 0.76$**

Figure 21. Lean Methane-Air Mixtures Stabilized with CAPAC Array

IV. Discussion and Future Work

The baseline experiment in this effort was designed to be similar in size and flowrate to the work conducted by Rajasegar et al. with coaxial microwave sources operating at 2.45 GHz [Rajasegar, 2017]. This work resulted in significant increase in the lean blowoff limit (LBO). These were however swirl stabilized flames with a swirling outer air flow in the range of 20 to 50 SLM. The premixed core flow consisted of 10 SLM air mixed with methane-air equivalence ratio in the range $\phi = 0.85$ to $\phi = 1.3$. Therefore, the core flow rates are similar to what has been applied for CAPAC-1B. Also, the CAPAC-1B achieves similar power levels to the microwave power which resulted in flame anchoring and improvement of OH radicals.

The LBO characteristics for the CAPAC-1B (0.5" outer tube) devices are somewhat similar to the low swirl flow cases for the microwave reactor, however, when the CAPAC center electrode is high up in the flow tube, an anchoring effect is achieved, allowing for a weak V-shaped flame to anchor for $\phi < \sim 1$ without plasma instead of an unstable flashback or LBO. For the CAPAC coax, it is certainly possible to develop cases with a marginally stable lifted flame for rich core flows, but there is no obvious similarity to the microwave swirl flow reactor cases operating with up to 50 SLM swirl flow [Rajasegar, 2017; Zimmerman et al. 2016b]. However, the flowrates of methane (and available heat release) are similar. When a smaller 0.25" outer tube was applied for the CAPAC-1G design, the anchoring dynamics were significantly changed, and the flashback leads to the flame quenching at $\phi < \sim 1$ even with the center electrode near the output. In this case, the effective tube diameter is closer to the quenching distance for methane in air, which is 2.5 mm (or 0.1"), and it is not possible to anchor a lean flame. For both the 0.25" and 0.5" tube sizes in CAPAC, the anchored shape is similar to that observed with the coaxial microwave when plasma is added, taking on a V-shape in the wake of the coax bluff body.

In future work, the NO_X emissions by CAPAC should be investigated. So far, preliminary measurements have been taken with a Stanford Research Systems QMS gas analyzer. However, there has been no indication of NO levels different from the flame without plasma, and lean operation regime has not yet been examined. There is some confidence that NO can be avoided based on examples with similar plasma torch-like devices, such as the DC plasmatron work by Rao et al. [Rao, 2009] where NO-PLIF was used. Applying a similar characterization and analysis to CAPAC would be useful in determining what environmental impact exists, and characterizing the behavior for the proposed commercial product. The work by Rao found that NO production was high for high currents and high power input, and in combination with lean mixtures. The typical plasma currents with CAPAC are at the low end of the current levels examined by Rao et al. where NO concentration for $\phi = 0.8$ was found to increase an order of magnitude from 500 ppm to 4500 ppm between 100 mA and 900 mA. The peak discharge currents for the Cyclotronic Arc Plasma Actuators (using similar driver circuits to the CAPAC devices here) are typically less than 100 mA [Zimmerman, 2019b], so it is anticipated that NO production can be maintained at a low level. However, more detailed study of lean operation and power to flow rate ratios is anticipated in future work along with NO_X characterization.

Although the CAPAC device here is a modification of the cyclotronic arc-plasma actuator (CAPA) [Ansell, et al., 2019], it is important to call attention to the magnetic gliding arc (MGA) device which have been investigated extensively for stabilization of counterflow diffusion flame burners [Ju et al., 2004; Ombrello et al., 2006; 2008]. While, the CAPAC is in principle a much simpler device in its configuration in comparison to the MGA instrument, the operating principles are similar, and there are potential advancements to be made for commercial combustion by reviewing and comparing to this work in detail. From the report by Ju et al. [Ju, 2004], the rotation of the arc in the MGA varied from 20 Hz to 50 Hz (1200 to 3000 RPM) for 30 to 90 W input power, and the rate decreased slightly

when the flow rate was increased from 1.83 LPM to 9.15 LPM (refer to Fig. 3 in [Ju et al., 2004]). These results can be compared directly to the high-speed visualization measurements above for the CAPAC-1B (see Figure 11) with the center electrode tip centered in the magnet (as in Figure 10a), where ~90 W input power resulted in 22,000 RPM in the zero-flow case, and reduced to approximately 17,000 RPM for flow rates between 6 and 15 LPM. However, placement of electrode in other orientations relative to the ring magnet resulted in significantly lower rotation (~5,200 RPM max) for placement near the upper surface (Figure 10b), or in the convergence point in the far field (Figure 10c). The difference seen here are most likely due to a combination of the placement of the arc in the *B*-field, and the driver circuit characteristics. In future study it is worth comparing the fundamental break down characteristics of the off-the-shelf Mazzilli-type ZVS driver circuit compared to the near-extinction piecewise discharge concept applied in the MGA driver [Ju, 2004].

For future work, CUA and UIUC plan to develop application-ready technologies utilizing magnetically-guided arc-plasma filaments for plasma-assisted combustion with a focus on a commercial prototype CAPAC array integrated with tankless water heat-exchanger. Key goals are demonstrating the extension of flammability limits, stability with lean operation, improved heat-release, and performance with infrastructure-compatible fuels. Improvements in practical operation of such devices is necessary for adoption in commercial products. Integration in formats and capacities similar to current commercial burners, with the plasma devices operated from conventional wall-plug power is an important step.

V. Conclusions

This initial research led to a variety of results about cyclotronic arc plasma assisted combustors (CAPACs) and key observations which will aid in future commercial development. Some of the important results of the investigations are as follows:

- The CAPAC bench tests were conducted with a compact circuit which can operate from either wall-plug or a 24-30 VDC source (i.e., easy to operate from solar power).
- Spectroscopic measurements showed both the breakdown of molecular gases by the plasma and modifications to the flame chemistry due to the plasma.
- PIV experiments (not detailed here, see [Hristov et al., 2022]) showed the impact of the plasma on the coaxial jet fluid dynamics (applied to a 0.5" diameter coax in air only). This experiment demonstrated the modification of the swirl-induced mixing in the jet above the CAPAC device.
- High speed imaging allowed characterization of the plasma arc filament due to Lorentz forcing for various arc-magnet arrangements, and showed the significant differences in rotation speed dependent on the positioning of the center electrode with respect to the ring magnet. These were compared to results in the literature for an MGA device used for diffusion flames. The CAPAC arrangement, with configuration of the arc break down inside the ring magnet was capable of significantly higher rotations rates, and similar rotation rates to the MGA when the arc was positioned near the upper surface, or in the far-field where the field lines converge. In all cases, flow and also combustion impact the character of the arc filament breakdown. A simple modification of the electrode configuration should enable strong high-speed rotation to be maintained.
- Schlieren imaging showed strong swirling induced in the flame zone, which is appealing for flame stability and mixing of air into the flame to promote efficiency.
- Application of the CAPAC during lean operation showed a significant decrease in the (unburnt) CO remaining above the flame. More detailed analysis of heat release and flow constituents in lean operation is required, and should be a key focus of future work.
- The CAPAC design could be applied in burners of various sizes and flow rates by adjusting the coaxial gap. The size of the burner could be adjusted over a wide range to accommodate various burner sizes, flow volumes, and operating regimes.

- An array of three CAPAC devices was assembled and bench tested. Operation of this design was demonstrated in cases which were typically unstable lean blow-off ($\phi = 0.76$). Plasma-assisted combustion with the array of CAPACs powered with a simple zero-voltage-switching DC-to-AC module and a modified CRT transformer enabled operation of flames at ($\phi = 0.76$) and available methane heat release from 46 kW to 138 kW for less than 200 W DC power supplied to the three ZVS modules. This serves as a starting point for further development of commercial burner components and heater prototypes in later phases which can supply significant heating in a compact burner, and a driver circuit that operates from household AC circuits.

This study provides initial foundation for application of magnetic gliding arc type devices in burners using natural gas sources, where an example is compact on-demand tankless water heaters. The 3-burner array developed in this study operated with between 46 kW and 138 kW available heat release (AHR) in the lean methane-air flow, with less than 200 W of total DC power applied to the plasma devices (the ratio of total DC input power to AHR was less than 0.4%). This available heating power is similar to the range of household and industrial on-demand heaters. For example, commercial natural gas tankless water heaters which operate in the range of 7 to 11 GPM provide 40 to 60 kW, similar to the range of the array developed in this study. Further work is needed to determine if this plasma actuator device could be applied to improve efficiency in on-demand heaters, while operating with low emissions of NO_X.

VI. Acknowledgements

This work was supported by DOE Small Business Innovative Research (SBIR) Grant # DE-SC0020814, and by CU Aerospace internal research and development funds. The authors wish to thank the DOE program manager Nirmol Podder for many helpful discussions about the research.

References

Ansell, P.J., Hristov, G., Zimmerman, J.W., and Carroll, D.L., "Cyclotronic Plasma Actuator with Arc-Magnet for Active Flow Control," United States Patent No. 10.332,724, 25 June 2019.

Barnard, J.A., and Bradley, J.N. "Flames and Combustion Waves," Flame and Combustion, Chapman and Hall Ltd., London, 1985 (2nd. Ed.), pp. 49-89.

Chakraborty, P., Balachandar, S., and Adrian, R, "On the Relationships Between Local Vortex Identification Schemes" 2005, Journal of Fluid Mechanics, Vol. 535, 189-214. https://doi:10.1017/S0022112005004726

Day, M.T., "Determining Gas Temperature from Spectroscopic Measurements in Electric Oxygen-Iodine Lasers," M.S. Thesis, Aerospace Engineering, University of Illinois at Urbana Champaign, (2011).

Gaydon, A.G., "Excitation of Metal Spectra in $H_2/O_2/N_2$ Flames," The Spectroscopy of Flames, Chapman and Hall Ltd., London, 1974 (2nd. Ed.), pp. 114-119.

Graves, D. B., and Kushner, M. J., "Low Temperature Plasma Science: Not Only the Fourth State of Matter but All of Them," Report of the DOE Office of Fusion Energy Sciences *Workshop on Low Temperature Plasmas March 25-27 2008* (2008)

Hammack, S., Rao, X., Lee, T., and Carter, C., "Direct-coupled Plasma-Assisted Combustion Using a Microwave Waveguide Torch," *IEEE Trans. Plasma Sci.*, Vol. 39, No. 12, pp. 3300-3306 (2011)

Hinsch, K. D., "Three-dimensional Particle Velocimetry," Meas. Sci. Tech., 6, pp. 742-753, 1995.

Hristov, G.K., P.J. Ansell, J.W. Zimmerman, and D.L. Carroll, "Experimental Characterization of a Novel Cyclotronic Plasma Actuator," AIAA Journal, online 15 Oct 2019, DOI 10.2514/1.J058708 (2019).

Hristov, G.K., et al., "Swirl Characterization of a Cyclotronic Arc Plasma Actuated Axial Air Jet" to be presented at AIAA SciTech 2022 (APA-76, Flow Control IX), San Diego, CA (2022)

Hunt, J., Wray, A., and Moin, P., "Eddies, Streams, and Convergence Zones in Turbulent Flows," Center for Turbulence Research, Proceedings of the Summer Program, Stanford Univ., Stanford, CA, 1988, pp. 193–202.

Ju, Y., Ombrello, T, Fridman, A., Gutsol, A., and Gangoli, S., "Enhancement of Combustion and Flame Stabilization Using Transient Non-Equilibrium Plasma," Final Report for Air Force Grant # FA9550-04-1-0038, 4 Jan. 2007

Kaufman, K.L., "Effect of hydrogen addition and burner diameter on the stability and structure of lean, premixed flames," Master of Science thesis, University of Iowa, 2014, DOI https://doi.org/10.17077/etd.h1cdxsj7
Kim, W., Snyder, J., and Cohen J., "Plasma assisted combustor dynamics and control," Proc. Comb. Inst. vol. 35, pp. 3479-3486 (2015)
Lee, D. H., Kim, K.-T., Cha, M. S., and Song, Y.-H., "Optimization scheme of a rotating gliding arc reactor for partial oxidation of methane," *Proc. Combust. Inst.*, **31** 3343-3351 (2007)
Londoño, L.F., et al., "Determination of laminar flame speed of methane-air flames at subatmospheric conditions using the cone method and CH* emission," Dyna, v. 80, no. 180, pp. 130-135, August 2013.
Mitsingas, C. M., R. Rajasegar, S. Hammack, H. Do, T. Lee, "High Energy Efficiency Plasma Conversion of CO_2 at Atmospheric Pressure Using a Direct Coupled Microwave Plasma System," IEEE Trans. Plasma Sci., Vol. 44, No. 4, pp. 651-656 (2016)
Ombrello, T, Qin, X., Ju, Y., Gutsol, A., Fridman, A., and Carter, C., "Combustion Enhancement via Stabilized Piecewise Non-Equilibrium Gliding Arc Plasma Discharge," AIAA Journal, Vol. 44, No. 1, 2006, pp. 142–150. doi:10.2514/1.17018
Ombrello, T, Ju, Y., and Fridman, A., "Kinetic Ignition Enhancement of Diffusion Flames by Nonequilibrium Magnetic Gliding Arc Plasma," AIAA Journal, Vol. 46, No. 10, 2008, pp. 2424–2433. doi:10.2514/1.33005
Power (online, 2020), "At the Dawn of the Hydrogen Economy," https://www.powermag.com/at-the-dawn-of-the-hydrogen-economy/
Prasad, A.K., Jensen, K., "Scheimpflug Stereocamera for Particle Image Velocimetry to Liquid Flows," Appl. Optics, 34, pp. 7092-7099, 1995.
Raffel, M., Willert, C., Kompenhans, J., "Particle Image Velocimetry: A Practical Guide," Springer-Verlag, Berlin, 1998, pp. 174–184.
Rajasegar, R., Mitsingas, C. M., Mayhew, E. K., Do, H., and Lee, T., "Effects of Continuous Volumetric Direct-Coupled Nonequilibrium Atmospheric Microwave Plasma Discharge on Swirl-Stabilized Premixed Flames," *IEEE Trans. Plasma Sci.*, Vol. 44, No. 1, pp. 39-48 (2016)
Rajasegar, R., Mitsingas, C. M., Mayhew, E. K., Yoo, J., and Lee, T., "Proper Orthogonal Decomposition for Flame Dynamics of Microwave Plasma Assisted Swirl Stabilized Premixed Flames," AIAA SciTech, 9-13 January 2017, Grapevine, Texas, AIAA 2017-1973 (2017)
Rao, X., Lee, T., and Matveev, I., "Nitric Oxide Formation during Ignition and Combustion of a Transient Arc Plasmatron," *47th AIAA Aerospace Sciences Meeting, 5-8 January 2009, Orlando, Florida*, AIAA-2009-280 (2009)
Rao, X., Hammack, S., Carter, C., Grotjohn, T., Asmussen, J., and Lee, T., "Microwave-Plasma-Coupled Re-Ignition of Methane-and-Oxygen Mixture Under Auto-Ignition Temperature," *IEEE Trans. Plasma Sci.*, Vol. 39, No. 12, pp. 3307-3313 (2011)
Rockwood, M. P., Taira, K., & Green, M. A., "Detecting Vortex Formation and Shedding in Cylinder Wakes Using Lagrangian Coherent Structures", 2017 AIAA Journal, 55(1), 15-23. https://doi.org/10.2514/1.J055051
Rothman, L.S., Gordon, I.E., Barbe, A., Benner, D.C., Bernath, P.F., et al., The HITRAN 2008 molecular spectroscopic database, J. of Quant. Spectros. & Radiat. Transfer, Vol. 110, pp. 533-572 (2009).
Zimmerman, J., Palla, A., King, D., Carroll, D., Mitsingas, C., Rajasegar, R., and Lee T., "Simulations of Plasma-Assisted Combustion Flames in Coaxial Microwave Reactors," AIAA SciTech, 4-8 Jan. 2016, San Diego, CA, AIAA-2016-0190 (2016a).
Zimmerman, J., Mitsingas, C., Rajasegar, R., Palla, A., King, D., Carroll, D., and Lee T., "Plasma-Assisted Methane Combustion in Swirled-Flow Reactors: Experiments and Multiphysics Simulations," AIAA Aviation, 13-17 June 2016, Washington, D.C., AIAA-2016-4139 (2016b).
Zimmerman, J.W., Palla, A.D., Carroll, D.L., Hristov, G.K., Ansell, P.J., "Plasma Actuator with Arc Breakdown in a Magnetic Field for Active Flow Control Applications," 48th AIAA Plasmadynamics and Lasers Conference, 5-9 June 2017, Denver, Colorado, AIAA Paper 2017-3477, (2017).
Zimmerman, J.W., Hristov, G.K., Ansell, P.J., and Carroll, D.L., "Development of a Plasma Actuator with Arc Breakdown in a Magnetic Field," AIAA Paper 2018-1555 (2018).
Zimmerman, J.W., G.K. Hristov, M. Vahora, M. Motz, D.R. Richardson, P.J. Ansell, and D.L. Carroll, "Scaling Studies of Cyclotronic Plasma Actuators for Active Flow Control Applications," AIAA Scitech 2019 Forum, San Diego, CA, 7-11 Jan. 2019, AIAA Paper 2019-0047, DOI, 10.2514/6.2019-0047 (2019a).
Zimmerman, J.W., G.K. Hristov, M. Vahora, P.J. Ansell, and D.L. Carroll, "Circuit Studies for Cyclotronic Plasma Actuators," AIAA Aviation 2019 Forum, 17-21 June 2019, AIAA Paper 2019-2997, DOI, 10.2514/6.2019-2997 (2019b).
Zimmerman, J.W., and Carroll, D.L., "Plasma Assisted Combustion Actuators with Arc Breakdown in a Magnetic

Field," AIAA Aviation 2019 Forum, 17-21 June 2019, AIAA Paper 2019-3120, DOI, 10.2514/6.2019-3120 (2019c).

AIAA SciTech Forum
January 3-7, 2022, San Diego, CA & Virtual
AIAA SCITECH 2022 Forum

10.2514/6.2022-2257.c1

Correction: Plasma-Assisted Burner Array Development using Cyclotronic Arc-Plasma Actuators

Author(s) Name: Joseph Zimmerman(1); David Carroll(1); Georgi Hristov(2); Phillip Ansell(2)
Author(s) Affiliations: 1. CU Aerospace LLC, Champaign, IL, United States. 2. University of Illinois at Urbana-Champaign, Urbana, IL, United States.

Correction Notice

The acknowledgements section of this paper (VI. Acknowledgements) should read as follows:

This work was supported by DOE Small Business Innovative Research (SBIR) Grant # DE-SC0020814, and by CU Aerospace internal research and development funds. The authors wish to thank the DOE program manager Nirmol Podder for many helpful discussions about the research. The authors also wish to thank John Halton-Berns for assistance with laboratory data collection and computer-aided design work for this project.